 doi:10.20944/preprints201812.0173.v1

Article

Synthesis, Crystal Structure, DFT studies, Docking Studies and Fluorescent Properties of 2-(Adamantan-1-yl)-2*H*-isoindole-1-carbonitrile

Jacques Joubert

Pharmaceutical Chemistry, School of Pharmacy, University of the Western Cape, Private Bag X17, Bellville, South Africa

* Correspondence: jjoubert@uwc.ac.za; Tel.: +27-21-959-2195

Abstract: 2-(Adamantan-1-yl)-2*H*-isoindole-1-carbonitrile (**1**) has been identified as a neurobiological fluorescent ligand that may be used to develop receptor and enzyme binding affinity assays. Compound **1** was synthesised using an optimised microwave irradiation reaction and crystallised from ethanol. Crystallization occurred in the orthorhombic space group $P2_12_12_1$ with unit cell parameters: a = 6.4487(12) Å, b = 13.648(3) Å, c = 16.571(3) Å, V = 1458(5) Å^3, Z = 4. Density functional theory (DFT) (B3LYP/6-311++G (d,p)) calculations of **1** were carried out. Results showed that the optimised geometry is similar to the crystal structure parameters with a root-mean-squared deviation of 0.143 Å. Frontier molecular orbital energies and net atomic charges are discussed with a focus on potential biological interactions. Docking experiments within the active site of the neuronal nitric oxide synthase (nNOS) protein crystal structure were carried out and analysed. Important binding interactions between the DFT optimised structure and amino acids within the nNOS active site were identified that explain the strong NOS binding affinity reported. Fluorescent properties of **1** were studied using aprotic solvents of different polarities. Compound **1** showed the highest fluorescence intensity in polar solvents with excitation and emission values of 336 nm and 380 nm, respectively.

Keywords: 2-(Adamantan-1-yl)-2H-isoindole-1-carbonitrile; X-ray diffraction; DFT; molecular orbital calculations; fluorescence; docking; nNOS; fluorescent ligand

1. Introduction

Radioligand binding techniques have been widely used to study biological proteins involved in the pathophysiology of neurodegenerative disorders such as Parkinson's disease and Alzheimer's disease [1-3]. Neuroprotective targets including the neuronal nitric oxide synthase (nNOS) enzyme [4], the *N*-methyl-D-aspartate (NMDA) receptor [3] and voltage gated calcium channels (VGCC) [5] have been widely studied using radioligands. Despite the usefulness and sensitivity of radioligand binding techniques the use of alternative approaches, such as fluorescent methods, to study receptor-ligand and enzyme-ligand binding interactions may provide information not readily accessible by conventional radiopharmacology. This will also circumvent some of the drawbacks, such as health hazards, high cost, disposal and potential technical implications, associated with radiopharmacology [6-9]. The development of small molecule fluorescent probes to study neurobiological events has thus become an area of intense interest [9,10]. Currently, there are no commercially available fluorescent ligands that are able to directly bind to the nNOS enzyme, NMDA receptor and/or VGCC, that can be used to develop binding affinity studies using fluorescent displacement assays.

2-(Adamantan-1-yl)-2*H*-isoindole-1-carbonitrile (1, Scheme 1) has shown ability to bind to and inhibit the nitric oxide synthase (NOS) enzyme [11], antagonise the *N*-methyl-D-aspartate (NMDA) receptor [12] and block voltage gated calcium channels (VGCC) [12]. Compound 1 also has inherent fluorescent properties because of the inclusion of the cyanoisoindole fluorophore in its structure

Preprints (www.preprints.org) | NOT PEER-REVIEWED | Posted: 14 December 2018 doi:10.20944/preprints201812.0173.v1

[11,13]. The ability of 1 to bind to these targets and show strong fluorescence may enable the design of a neurobiological fluorescent ligand that could be used to develop receptor and enzyme binding affinity assays. This study therefore set out to improve the synthesis of 1, study its crystal structure and geometry in both solid and free form state, analyse the frontier molecular orbitals and atomic net charges, perform docking experiments to elucidate the potential biological binding interactions and further explore its fluorescent properties. These studies will provide valuable information that may be used to develop fluorescent displacement assays utilising compound 1.

2. Results and Discussion

2.1. Chemistry

2-(Adamantan-1-yl)-2H-isoindole-1-carbonitrile (**1**) was obtained through the reaction of *o*-phthaldialdehyde (OPD) with amantadine.HCl in the presence of sodium cyanide under optimised microwave (MW) irradiation (150 W, 100 °C, 150 psi) conditions (Scheme 1). Both OPD and amantadine.HCl are commercially available. The reaction proceeded efficiently providing the title compound in an excellent yield of 91% after only 10 minutes of reaction time. This is a significant improvement in yield and reduction in reaction time compared to the conventional method previously described where a yield of 66% was obtained with a reaction time of 24 hours [12]. The molecular structure was confirmed by ^{1}H and ^{13}C nuclear magnetic resonance (NMR), high-resolution mass spectroscopy and X-ray diffraction.

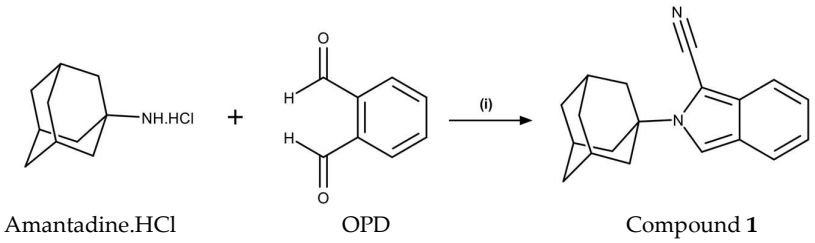

Amantadine.HCl OPD Compound **1**

Scheme 1. Reagents and conditions for the synthesis of 2-(adamantan-1-yl)-2H-isoindole-1-carbonitrile (**1**): (i) MeOH, NaCN, H_2O, MW, 150 W, 100 °C, 150 psi, 10 min, 91% yield.

2.2. Crystal Structure and Geometry Optimization

A crystalline material was grown from EtOH at room tempreture for 24 hours. The rod-like crystal crystallises in the orthorhombic space group $P2_12_12_1$. The asymmetric unit cell of the title compound contains four molecules. The molecular structure is shown in Figure 1, and the packing diagram is in Figure 2a and 2b. Selected bond lengths and bond angles are listed in Table 1.

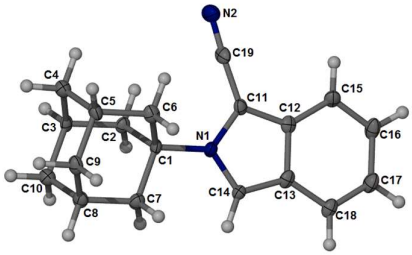

Figure 1. The asymmetric unit of compound **1** showing the atomic numbering scheme and 30% probability displacement ellipsoids of non-H atoms.

Bond lengths, angles and torsion angles of the adamantane ring system is consistent with other previously published structures [14]. The geometry of the cyano group is within the normal range for nitriles. Generally, the bond lengths and bond angles of the isoindole structure are very similar as those reported for N-methylisoindole [15], suggesting that substitutions to the pyrrolidine ring at the

Preprints (www.preprints.org) | NOT PEER-REVIEWED | Posted: 14 December 2018 doi:10.20944/preprints201812.0173.v1

C11 position do not significantly alter the solid-state geometry. The orientation of the cyanoisoindole moiety in relation to the adamantane moiety is defined by the bond angles of C1-N1-C11 (124.63°) and C1-N1-C14 (126.56°), and the torsion angles of C1-N1-C11-C12 (-177.56°) and C1-N1-C14-C13 (178.93°). The crystal packing is not planar and has an inversion-related molecular arrangement. An intermolecular hydrogen bond is observed at C2-H2A···N2. The D···A distance is 2.61 Å and the D-H···A angle is 161° Å. The formation of the self-assembled crystal structure can also be attributed to a number of weak C-H···π interactions between the adamantane and the isoindole moieties of the molecules constituting the crystal assembly (Figure 2b). Thus, the crystal structure is built up through a combination of hydrogen bond and C-H···π interactions.

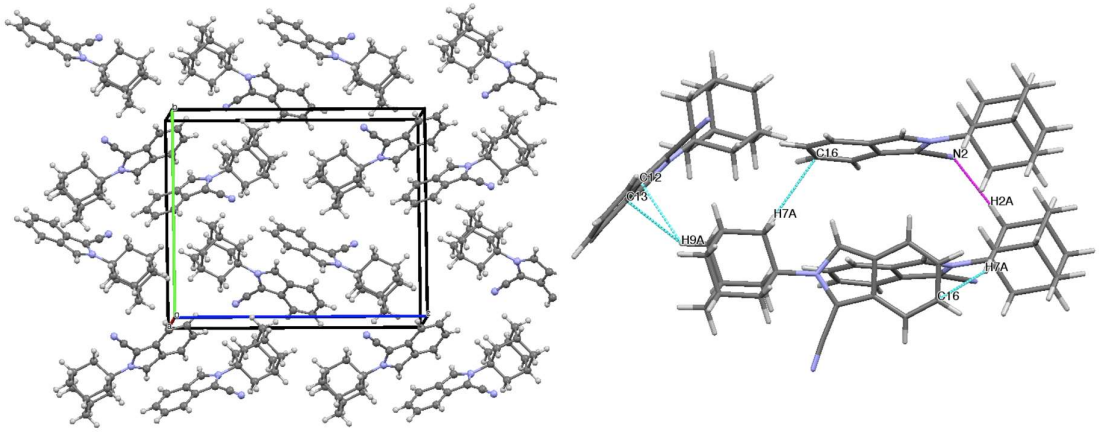

(a) **(b)**

Figure 2. (a) The molecular crystal packing of compound **1** viewed along the b-axis. (b) Partial crystal packing showing the H-bond (magenta) and C-H···π (light blue) intermolecular interactions along the c-axis.

A density functional theory (DFT) geometry optimisation of **1** was performed with the Gaussian09 program package [16] employing Becke's three parameters Lee–Yang–Parr exchange correlation functional (B3LYP), which combines the hybrid exchange functional of Becke [17] with the gradient-correlation functional of Lee, Yang and Parr [18] using the 6-311G++(d,p) basis set. No solvent corrections were made with these calculations as it was reported that gas phase calculations frequently correspond quite well with crystal structures [19]. The X-ray refined data was used to select a crystal unit containing the starting geometries of compound **1**. The geometry of compound **1** was optimised and the DFT optimised molecule was generated. Table 1 contains the data comparing the experimental with the calculated structure of **1**.

The C–C bond lengths within the isoindole structure is in the range of 1.41–1.42 Å and 1.42–1.43 Å for the experimental X-ray structure and at the calculated B3LYP/6-311G++(d,p) level, respectively, which is much shorter than characteristic C-C single bonds (1.54 Å) [20]. The experimental (1.36-1.40 Å) and calculated (1.37-1.41 Å) C-C bonds of the adamantane structure are within the reported characteristic range [14]. The C=C bonds were found to be slightly longer than normal C=C bond lengths (1.34 Å) [20] for both the experimental (1.52-1.54 Å) and calculated (1.53-1.55 Å) results. For N2-C19 the calculated C≡N (nitrile) bond length is 1.16 Å which is longer than the experimental value of 1.14 Å and is exactly the same as the bond length (1.16 Å) described for nitriles in chemistry literature. The N1–C1, N1–C11 and N1–C14 bond lengths are calculated as 1.50, 1.40 and 1.36 Å at the B3LYP/6-311G level and experimental values are 1.49, 1.39 and 135 Å, respectively. It is noted that the N1–C11 and N1–C14 bond lengths are much shorter than the normal C–N bond length (1.47 Å) while N1–C1 is closer to the normal length. The shorter N1–C11 and N1–C14 bond lengths observed is because they are part of the unconjugated isoindole structure. These bond lengths are consistent with similar isoindole structures reported in the literature [15]. The bond angles calculated are in good agreement with the experimental data with a maximum deviation of 1.26° for C1–N1–C14,

Preprints (www.preprints.org) | NOT PEER-REVIEWED | Posted: 14 December 2018 doi:10.20944/preprints201812.0173.v1

which is calculated as 125.31° and the experimental value is 126.57°. The largest deviation between bond lengths is 0.025 Å for N2-C19.

Table 1. Bond lengths (Å), angles (°) and theoretical calculations for the title compound.

Bond Lengths (Å)	X-ray crystal	DFT[a]	Bond Angles (°)	X-ray crystal	DFT[a]
N1-C14	1.352	1.360	C14-N1-C11	108.77	109.13
N1-C1	1.498	1.499	C1-N1-C14	126.57	125.31
N1-C11	1.389	1.395	C2-C3-C10	110.53	109.52
N2-C19	1.136	1.161	C10-C3-C4	110.10	109.74
C3-C10	1.520	1.539	N1-C1-C2	109.54	109.72
C1-C2	1.531	1.548	C2-C1-C6	110.85	110.21
C11-C12	1.397	1.408	C6-C1-C7	108.39	108.39
C12-C13	1.433	1.433	C11-C12-C13	106.98	106.78
C13-C18	1.412	1.417	C11-C12-C15	132.27	132.92
C5-C6	1.526	1.542	C13-C12-C15	120.67	120.30
C15-C16	1.375	1.375	N1-C11-C12	107.88	107.88
C16-C17	1.408	1.425	N1-C11-C19	125.49	125.69
			C13-C18-C17	118.66	118.44
			N2-C19-C11	176.20	176.79
			C12-C15-C16	117.31	118.21
			C15-C16-C17	122.20	121.68

[a]DFT optimisation was performed at B3LYP/6-311++G(d,p) level.

These deviations between bond lengths and bond angles, although relatively minor, are because the calculations belong to the gaseous phase and the experimental results belong to the solid phase. In the solid state, the crystal field along with the intermolecular interactions has linked the molecules together, which results in the difference in bond parameters between the experimental and calculated values. Overlay analysis was performed using YASARA version 18.11.21 (YASARA Biosciences GmbH) to globally compare the structure obtained with the theoretical calculation with that obtained from the X-ray diffraction (Figure 3). A relatively low root-mean-squared deviation (RMSD) value of 0.143 Å was obtained confirming that there are minor differences between the calculated and experimental structures.

Figure 3. Atom-by-atom superimposition of DFT optimised compound **1** (magenta) calculated using B3LYP/6-311++G (d,p) on the X-ray structure (blue) of **1** (RMSD = 0.143 Å).

2.3. Frontier Molecular Orbitals and Atomic Net Charges

The most significant orbitals in molecules are the frontier molecular orbitals, called the Highest Occupied Molecular Orbital (HOMO) and the Lowest Unoccupied Molecular Orbital (LUMO). HOMO has the ability to donate an electron, and LUMO, as an electron acceptor, has the ability to obtain an electron [21]. According to the frontier molecular orbital theory, HOMO and LUMO are important factors that affect the bioactivity, chemical reactivity, electron affinity and ionisation potential [22-27]. Thus, the study on the frontier orbital energy can provide valuable information with

Preprints (www.preprints.org) | NOT PEER-REVIEWED | Posted: 14 December 2018 doi:10.20944/preprints201812.0173.v1

respect to biological mechanisms. Figure 4 shows the distribution and energy levels of HOMO and LUMO orbitals computed at the B3LYP/6-311G level for the title compound **1**.

As can be seen from Figure 4, both the LUMO and HOMO is mainly localised at the nitrile and isoindole moieties. This indicates that the activity associated with this molecule could generally be attributed to the cyanoisoindole structure with the adamantane moiety mostly providing structural bulk and/or lipophilic function. This finding is in line with hypotheses from previous studies [11, 12]. It is thus postulated, based on HOMO and LUMO findings, that the cyanoisoindole structure will form interactions with amino acids lining the active sites of the NOS enzyme, NMDA receptor and/or VGCC and in so doing give rise to its reported biological activity.

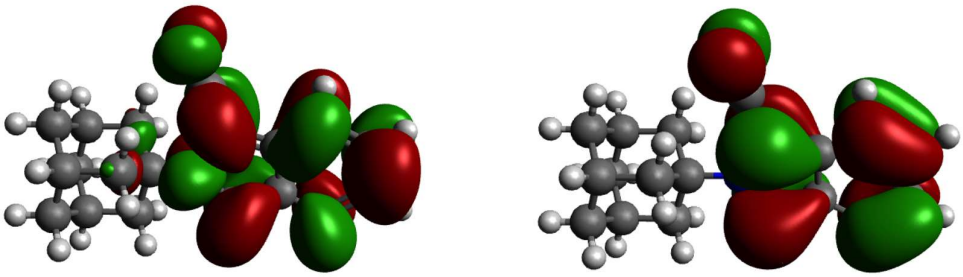

LUMO (-1.550 eV) HOMO (-5.625 eV)

Figure 4. The frontier molecular orbitals of compound **1** calculated using B3LYP/6-311++G (d,p).

The atomic net charges of the DFT optimised structure are shown in figure 5. The two N-atoms have the highest electronegativity and showed the lowest net atomic charge values (N1 = -0.32 e and N2 = -0.19 e) within the structure of **1**. Therefore, it is expected that the N-atoms will be the most favored to interact with positively charged amino acids within the enzyme and receptor active sites. However, even though the N1 atom showed a lower net atomic charge compared to N2 it will encounter some difficulty to form interactions with amino acids because of the structural hindrance imposed by the bulky adamantane group. Therefore, interactions are expected to be present at the N2 position because the nitrile group is protruding outwards from the isoindole structure and should present with an effective handle for interactions to take place.

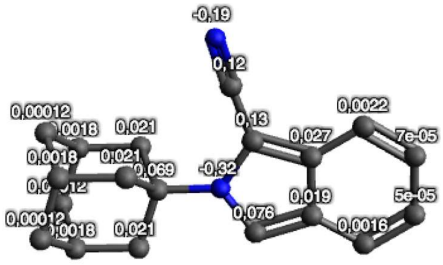

Figure 5. The atomic net charges (e) of the DFT optimised structure of **1**. Hydrogens are not shown.

2.4. Docking studies

Molecular modelling studies using the NMDA receptor and VGCC were not carried out because the full protein crystal structure of these targets have not yet been published. Therefore, in order to further explore the interaction profile and biological potential/application of **1**, molecular docking studies were performed using the crystal structure (Protein Data Bank I.D.: 1OM5) of rat nNOS co-crystallised with the known nNOS inhibitor 3-bromo-7-nitroindazole (3B7NI) [28] (Figures 6 and 7). 3B7NI crystallised in the active heme (HEM750) site domain of nNOS.

Preprints (www.preprints.org) | NOT PEER-REVIEWED | Posted: 14 December 2018 doi:10.20944/preprints201812.0173.v1

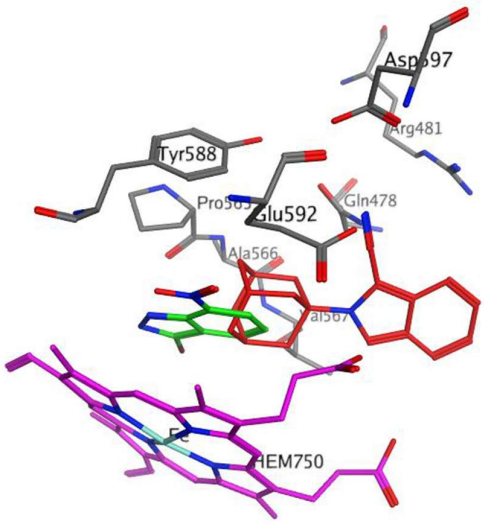

Figure 6. The putative binding modes and orientation of 3B7NI (green) and compound **1** (red) within the rat nNOS heme domain active site. The heme cofactor (HEM750) is shown in magenta and the surrounding amino acids are shown in grey.

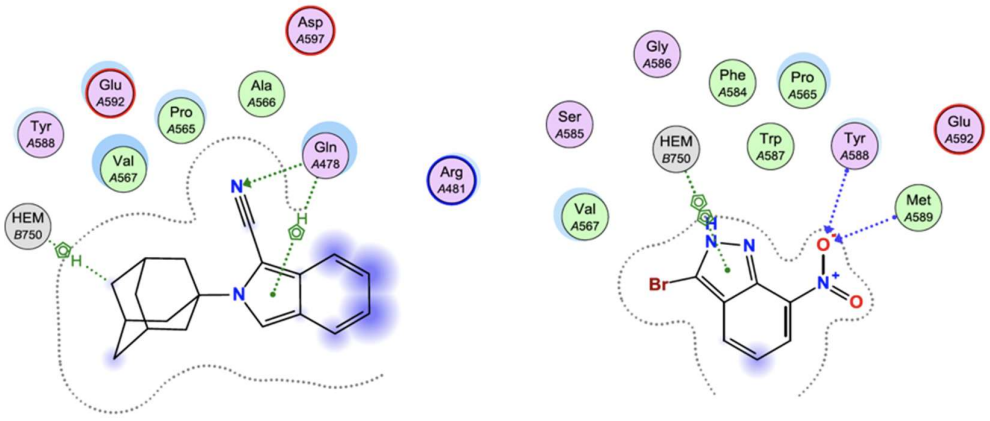

Binding affinity (**1**) = -5.722 kcal/mol Binding affinity (**3B7NI**) = -6.000 kcal/mol

Figure 7. Binding interactions and binding affinity (kcal/mol) of compound **1** and the co-crystallised ligand, 3B7NI, within the active site of the nNOS heme domain.

Inspection of the binding mode of 3B7NI indicated that two hydrogen bond contacts are formed through the interaction of the 7-NO_2 moiety with residues Tyr588 and Met589 (Figure 7). A π-π interaction was also observed between the pyrazole ring of the indazole structure and HEM750. These interactions within the active site could be responsible for the potent nNOS inhibitory activity reported for 3B7NI (rat nNOS IC_{50} = 0.17 μM) [28]. The binding affinity of 3B7NI was found to be -6.000 kcal/mol. The DFT optimised (B3LYP/6-311++G (d,p)) structure of **1** was used for further docking studies (Figure 7). Compound **1** was docked using the protocol as described in the experimental section and was able to access and bind to the active heme site domain of nNOS, similar to 3B7NI. Two H-π interactions were observed between the adamantane moiety and HEM750 and between Gln478 and the pyrrolidine ring of the isoindole structure. Compound **1** also showed a hydrogen bond interaction between the electornegative nitrile moiety and Gln478. This result is as expected based on the frontier molecular orbital and net atomic charges findings. The binding affinity of **1** was found to be -5.722 kcal/mol. The binding interactions and binding affinity of **1**, which is similar to 3B7NI, may be the reason for the significant NOS inhibitory activity reported (rat NOS IC_{50}

 doi:10.20944/preprints201812.0173.v1

= 0.29 μM) [12]. A virtual derivative of **1** devoid of the nitrile group was also docked and showed no binding interactions within the active site. This finding demonstrates the importance of the nitrile moiety in this structure for nNOS inhibitory activity. In addition, no covalent intermolecular biological interactions were identified suggesting that this molecule will be suited for fluorecent displacement studies to determine binding affinity of test compounds.

It is important to note that **1** has only been evaluated on a crude NOS extract [12] containing the inducible-, endothelial- and neuronal NOS isoforms and further biological studies are necessary in order determine the NOS isoform selectivity profile of this compound. However, this docking study indicates that **1** should show significant nNOS inhibitory activity which is vital in order to treat neurodegenerative disorders or to develop molecular probes for neurobiological studies.

2.5. Fluorescent Properties

The excitation and emission spectra of compound **1** recorded in a dimethyl sulfoxide (DMSO) solution (1 x 10^{-5} mol/L) is shown in Figure 8a. A BioTek Synergy fluorescent plate reader was used for all fluorescence measurements. The excitation absorption maximum and the emission maximum were found to be 336 nm and 380 nm, respectively. The strong emission can be explained by comparing the fluorecent properties of the 1-nitrile substituted compound **1** with that of a reported unsubstituted N-methylisoindole compound (emission = 345 nm) [15]. When the electron-withdrawing nitrile group is present the charge separation of the molecule is enhanced due to an internal Stark effect [29,30] which, in turn, results in a red-shift in the fluorescence spectrum and increase in fluorecence intensity [31]. Therefore, the nitrile moiety is of significant importance in order for compound **1** to show strong fluorescent properties.

Figure 8b shows the influence of different aprotic solvents of varying polarities on the emission spectra of compound **1** (1 x 10^{-5} mol/L). No noticeable shift in the emission value of **1** was observed in the different solvents. The results, however, indicate that the solvent polarity had a profound effect on the emission intensity of **1**. The fluorescence intensity significantly decreased as the polarity of the solvents decreased (Figure 8b). This initial study indicates that **1** exhibits a solvatochromic effect in the different solvents with varying polarity, most probably due to an internal charge transfer phenomenon.

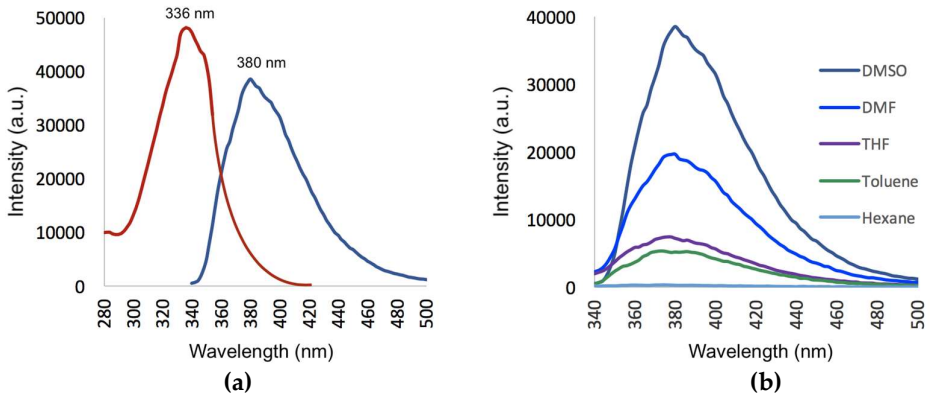

Figure 8. (a) Excitation and emission specta of compound **1**. (b) Fluorescent spectra of compound **1** showing the effect of different aprotic solvents of varying polarities.

Fluorescent properties of the solid crystalline state of **1** was also determined. Interestingly, a definite red shift was observed for both the excitation (336 nm to 346 nm) and emission (380 nm to 400 nm) for the solid-state of **1**. In the solid state there are intermolecular interactions present between the molecules in the crystal field (see Figure 2b). These interactions altered the physical and chemical properties which led to a change in the photochemical properties of **1** compared to when the compound is dissolved in organic solvents and intermolecular bonds are broken.

Preprints (www.preprints.org) | NOT PEER-REVIEWED | Posted: 14 December 2018 doi:10.20944/preprints201812.0173.v1

3. Materials and Methods

3.1. Chemistry

3.1.1. General information

Unless otherwise specified, all chemicals were obtained from Sigma-Aldrich or Merck. All the chemicals were of analytical grade and used without further purification. Compound **1** was characterised using nuclear magnetic resonance (NMR) and high resolution mass spectrometry (HRMS) techniques. NMR's were obtained using a Bruker 400 MHz instrument. The chemical shifts are reported as δ values in ppm downfield from tetramethylsilane as internal standard. Deuterated chloroform ($CDCl_3$) was used as NMR solvent. The multiplicities of NMR signals are expressed as: s, singlet or m, multiplet. HRMS was recorded on a Waters API Q-Tof Ultima electro-spray ionisation mass spectrometer at 70 eV and 100 °C. The melting point was determined using a Stuart SMP-10 melting point apparatus. The melting point is uncorrected. Microwave synthesis was performed using a CEM Discover™ focused closed vessel (maximum capacity = 30 ml) microwave synthesis system.

3.1.2. Synthesis of 2-(adamantan-1-yl)-2H-isoindole-1-carbonitrile (1)

Amantadine hydrochloride (0.600 g, 3.301 mmol) and sodium cyanide (NaCN, 0.132 g, 3.301 mmol) was dissolved in 15 ml methanol. Distilled water (1 mL) and *o*-phthaldialdehyde (0.442 g, 3.301 mmol) were added. The reaction mixture was placed in the microwave reactor and irradiated at 150 W, 100 °C and 150 psi for 10 minutes. Upon cooling in an ice bath a white precipitate formed and was filtered and washed twice with cold methanol (10 ml) and twice with distilled water (10 ml) to yield the pure product (1) as a white amorphous solid in high yield (0.828 g, 2.997 mmol, 91%). Further crystallization by slow diffusion of a solution in EtOH was carried out to provide a rod-like single crystal suitable for X-ray diffraction analysis. Mp: 160 °C; ^{1}H NMR (400 MHz, $CDCl_3$) δ_H: 7.69–7.64 (m, 2H), 7.51 (s, 1H), 7.26–7.19 (m, 1H), 7.12–7.04 (m, 1H), 2.45 (m, 6H), 2.32 (s, 3H), 1.85-1.80 (m, 6H); ^{13}C NMR (100 MHz, $CDCl_3$) δ_C: 150.6, 133.9, 125.3, 122.7, 122.4, 120.9, 117.8, 116.6, 115.9, 60.4, 43.00, 35.9, 30.0; HRMS m/z: Calculated for $C_{19}H_{20}N_2$ (M+H); 276.16366, found 276.16265.

3.2. X-ray crystallography

Single-crystal X-ray intensity data were collected on a Bruker 3-circle Apex II DUO X-ray diffractometer equipped with an INCOATEC IμS HB microfocus sealed tube (MoKα radiation λ = 0.71073 Å) fitted with a multilayer monochromator. Data were captured with a charge-coupled device (CCD) area detector. Data collection was carried out at 100 K using an Oxford Cryosystems cryostat (700 series Cryostream Plus) attached to the diffractometer. Data collection and reduction were carried out using the Bruker software package APEX3 [32], using standard procedures. All structures were solved and refined using SHELX-2016 [33] employed within the X-Seed [34,35] environment. Hydrogen atoms were placed in calculated positions using riding models. Table 2 contains the crystal data and refinement parameters.

A CIF file containing complete information of the studied structure was deposited with CCDC, deposition number 1881043 and is freely available upon request from the Director, CCDC, 12 Union Road, Cambridge CB2 1EZ, UK (Fax: +44-1223-336033; e-mail: deposit@ccdc.cam.ac.uk) or from the following website: www.ccdc.cam.ac.uk/data_request/cif.

Table 2. Crystal data and refinement parameters of the tile compound **1**.

Crystal data	**1**
Chemical formula	$C_{19}H_{20}N_2$
M_r	276.37
Crystal system, space group	Orthorhombic, $P2_12_12_1$
Temperature (K)	100

 doi:10.20944/preprints201812.0173.v1

a, b, c (Å)	6.4487 (12), 13.648 (3), 16.571 (3)
V (Å^3)	1458.4 (5)
Z	4
Radiation type	Mo $K\alpha$
μ (mm^{-1})	0.07
Crystal size (mm)	0.59 × 0.05 × 0.05
Diffractometer	Bruker *APEX* II DUO CCD
T_{min}, T_{max}	0.931, 1.000
No. of measured, independent and observed [$I > 2\sigma(I)$] reflections	14040, 3372, 2528
R_{int}	0.072
(sin θ/λ)$_{max}$ (Å^{-1})	0.650
$R[F^2 > 2\sigma(F^2)]$, $wR(F^2)$, S	0.074, 0.199, 1.04
No. of reflections	3372
No. of parameters	190
Δϱ$_{max}$, Δϱ$_{min}$ (e Å^{-3})	0.69, −0.28

3.3. Theoretical Calculations

According to the crystal structure of **1**, a crystal unit was selected as the initial structure, while DFT-B3LYP/6-311G++(d,p) methods in Gaussian09 [16] was used to optimise the structure of the title compound. No solvent corrections were made with these calculations. Vibration analysis showed that the optimised structure indeed represents a minimum on the potential energy surface (no negative eigenvalues). For the optimised structure, the HOMO and LUMO were drawn using Avogadro 1.2.0 [36,37]. Atomic net charges were also calculated using Avogadro 1.2.0.

3.4. Docking studies

The docking studies were performed using the rat nNOS heme domain crystal structure (Protein Data Bank I.D.: 1OM5). The Molecular Operating Environment (MOE) 2018 software suite [38] was used for docking studies with the following protocol. (1) The enzyme protein structure was checked for missing atoms, bonds and contacts. (2) Removal of water molecules, 3D protonation and energy minimization was carried out with parameters, force field: MMFF94X+solvation, gradient: 0.05, chiral constraint and current geometry. This minimised structure was used as enzyme for docking analysis. (3) The DFT B3LYP/6-311++G (d,p) optimised structure of **1** was saved as a pdb file and imported into the MOE database. (4) Compound **1** was subsequently docked within the nNOS heme domain active site using the MOE Dock application. The active site was selected based on the proximity of the co-crystallised ligand, 3B7NI, with the help of the MOE Site Finder tool. The docking algorithm which was chosen for these experiments were based on induced fit docking to allow for flexible interactions of the test ligand with the protein. (5) The best binding pose of compound **1** was visually inspected and the interactions with the binding pocket residues were analysed. The selected parameters that were used to calculate the score and interaction of the ligand molecule with the nNOS enzyme were; Rescoring function: London dG, Placement: Triangle matcher, Retain: 30, Refinement: Force field, Rescoring 2: London dG. The build-in scoring function of MOE, S-score, was used to predict the binding affinity (kcal/mol) of the ligand with the enzyme protein active site after docking.

4. Conclusions

2-(Adamantan-1-yl)-2H-isoindole-1-carbonitrile (1) was synthesised using an optimised microwave irradiation synthesis method in high yield. The three-dimensional structure of 1 was confirmed by single crystal X-ray diffraction. Using DFT calculations at the B3LYP level of theory and the 6-311G++(d,p) basis set, the molecular structure and electronic properties of 1 were deduced. Molecular docking studies indicated important interactions of 1 with the active site of the nNOS

enzyme and showed that the nitrile moiety is imperative for nNOS inhibitory activity. The fluorescent properties of 1 were studied and strong fluorescence was shown at 380 nm in polar aprotic solvents.

This study has therefore provided valuable information of 1 that may be used to develop a pharmacological tool to investigate enzyme–ligand and/or receptor–ligand interactions utilising modern fluorescent imaging techniques.

Funding: This research was funded by the National Research Foundation (NRF, South Africa, Grant Number: 11181) and the University of the Western Cape.

Acknowledgments: Prof. E. Antunes from the Chemistry Department of the University of the Western Cape is acknowledged for NMR data collection. Dr L. Loots from the Chemistry and Polymer Science Department of Stellenbosch University is acknowledged for the X-ray diffraction data collection and analysis. The Centre for High Performance Computing at the Council for Scientific and Industrial Research (South Africa) is acknowledged for granting access to Gaussian09 software.

Conflicts of Interest: The author declares no conflict of interest.

References

1. Laruelle, M. (2000). Imaging synaptic neurotransmission with in vivo binding competition techniques: A critical review. J. Cereb. Blood Flow Metab. 2000, 20(3), 423–451.
2. Kreisl, W.C.; Lyoo, C.H.; McGwier, M.; Snow, J.; Jenko, K.J.; Kimura, N.; Corona, W.; Morse, C.L.; Zoghbi, S.S.; Pike, V.W.; McMahon, F.J.; Turner, R.S.; Innis, RB. *In vivo* radioligand binding to translocator protein correlates with severity of Alzheimer's disease. Brain. 2013, 136(7), 2228–2238.
3. Geldenhuys, W.J.; Terre'Blanche, G.; Van der Schyf, C.J.; Malan, S.F. Eur. J. Pharmacol. 2003, 458, 73-79.
4. Mayer, B.; Klatt P.; Werner, E.R.; Schmidt, K. Identification of imidazole as l-arginine-competitive inhibitor of porcine brain nitric oxide synthase. FEBS Lett, 1994, 350, 199-202.
5. Zheng, W. Characterization of aclcium channel binding. Curr. Prot. Pharmacol. 2001, 14, 1.25.1-1.25.12.
6. Auer, M.; Moore, K.J.; Myers-Almes, F.J.; Guenther, R.; Pope, A.J.; Stoekli, K.A. Fluorescence correlation spectroscopy: lead discovery by miniaturized HTS. Drug Discov. Today. 1998, 3, 457-465.
7. McGrath, J.C.; Arribas, S.; Daily, C.J. Fluorescent ligands for the study of receptors. Trends Pharmacol. Sci. 1996, 17, 393-399.
8. McCabe, R.T.; Newman, A.H.; Skolnick, P. AHN 683: a fluorescent ligand for peripheral-type benzodiazepine receptors. J. Pharmacol. Exp. Ther. 1992, 262, 734-740.
9. Joubert, J.; van Dyk, S.; Malan, S.F. Small molecule fluorescent ligands as central nervous system imaging probes. Mini-Rev. Med. Chem. 2013, 13(5), 682-696.
10. McCarron, S.T.; Chambers, J.J. Modular chemical probes for visualizing and tracking endogenous ion channels. Neuropharmacol. 2015, 98, 41-47.
11. Joubert, J.; van Dyk, S.; Malan, S.F. Fluorescent polycyclic ligands for nitric oxide synthase (NOS) inhibition. Bioorg. Med. Chem. 2008, 16(19), 8952-8958.
12. Joubert, J.; Dyk, S.V.; Green, I.R.; Malan, S.F. Synthesis and evaluation of fluorescent heterocyclic aminoadamantanes as multifunctional neuroprotective agents (2011). Bioorg. Med. Chem. 2011, 19(13), 3935-3944.
13. Joubert, J.; Dyk, S.V., Green, I.R., Malan, S.F. Synthesis, evaluation and application of polycyclic fluorescent analogues as N-methyl-d-aspartate receptor and voltage gated calcium channel ligands. Eur. J. Med. Chem. 2011, 46(10), 5010-5020.
14. Joubert, J.; Samsodien, H.; Baber, Q.R.; Cruickshank, D.L.; Caira, M.R.; Malan, S.F. Synthesis and structural analysis of novel neuroprotective pentacyclo[5.4.1.02,6.03,10.05,9]undecane- and adamantane-derived propargylamines. J. Chem. Cryst. 2014, 44(4), 194-204.
15. Jones, G.B.; Chapman, B.J.; 2.01 - Pyrroles and their Benzo Derivatives: Structure.; Katritzky, A.R.; Rees, C.W.; Scriven, E.F.V. In Comprehensive Heterocyclic Chemistry II, Pergamon, Oxford, United Kingdom, 1996; pp. 1-38, ISBN 9780080965185.
16. Frisch, M.J.; Trucks, G.W.; Schlegel, H.B.; Scuseria, G.E.; Robb, M.A.; Cheeseman, J.R.; Scalmani, G.; Barone, V.; Mennucci, B.; Petersson, G.A.; et al. Gaussian 09; Gaussian, Inc.: Wallingford, CT, USA, 2009.
17. Becke, A.D. Density-functional exchange-energy approximation with correct asymptotic behavior. Phys. Rev. A 1988, 38, 3098.

18. Lee, C.; Yang, W.; Parr, R.G. Development of the colle-salvetti correlation-energy formula into a functional of the electron density. Phys. Rev. B 1988, 37, 785.
19. Honarparvar, B.; Govender, T.; Maguire, G.E.; Soliman, M.E.; Kruger, H.G. Integrated approach to structure-based enzymatic drug design: Molecular modeling, spectroscopy, and experimental bioactivity. Chem. Rev. 2013, 114, 493–537.
20. Lide, D.R. A survey of carbon-carbon bond lengths. Tetrahedron. 1962, 17, 125–134.
21. Becker, H. Jan Fleming, Frontier Orbitals and Organic Chemical Reactions., John Wiley u. Sons LTD. J. Praktische Chem. 1978, 320, 879–880.
22. Contreras, R.; Domingo, L.R.; Andrés, J.; Pérez, P.; Tapia, O. Nonlocal (pair site) reactivity from second-order static density response function: Gas-and solution-phase reactivity of the acetaldehyde enolate as a test case. J. Phys. Chem. A. 1999, 103, 1367–1375.
23. Clare, B.W. Frontier orbital energies in quantitative structure-activity relationships: A comparison of quantum chemical methods. Theor. Chim. Acta 1994, 87, 415–430.
24. Clare, B.W. The relationship of charge transfer complexes to frontier orbital energies in qsar. J. Mol. Struct. Theochem. 1995, 331, 63–78.
25. Clare, B.W. Charge transfer complexes and frontier orbital energies in qsar: A congeneric series of electron acceptors. J. Mol. Struct. Theochem. 1995, 337, 139–150.
26. Heaton, C.; Miller, A.; Powell, R. Predicting the reactivity of fluorinated compounds with copper using semi-empirical calculations. J. Fluor. Chem. 2001, 107, 1–3.
27. Zhang, G.; Musgrave, C.B. Comparison of DFT methods for molecular orbital eigenvalue calculations. J. Phys. Chem. A. 2007, 111, 1554–1561.
28. Claramunt, R.M.; López, C.; Pérez-Medina, C.; Pérez-Torralba, M.; Elguero, J.; Escames, G.; Acuña-Castroviejo, D. Fluorinated indazoles as novel selective inhibitors of nitric oxide synthase (NOS): Synthesis and biological evaluation. Bioorg. Med. Chem. 2006, 17(17), 6180-6189.
29. Callis, P.R.; Burgess B.K. Tryptophan Fluorescence Shifts in Proteins from Hybrid Simulations: An Electrostatic Approach. J. Phys. Chem. B. 1997, 101, 9429–9432.
30. Vivian, J.T.; Callis, P.R. Mechanisms of tryptophan fluorescence shifts in proteins. Biophys J. 2001, 80, 2093–2109.
31. Hilaire MR, Mukherjee D, Troxler T, Gai F. Solvent Dependence of Cyanoindole Fluorescence Lifetime. Chem. Phy.s Lett. 2017, 685, 133-138.
32. APEX3, SAINT, and SADABS; Bruker AXS Inc.: Madison, WI, 2018.
33. Sheldrick, G.M., Crystal structure refinement with SHELXL. *Acta Cryst*., 2015, C71, 3-8.
34. Atwood, J.L.; Barbour, L.J. Molecular Graphics: From Science to Art. Cryst. Growth Des. 2003, 3, 3−8.
35. Barbour, L.J. X-Seed — A Software Tool for Supramolecular Crystallography. J. Supramol. Chem. 2001, 1, 189−191.
36. Avogadro: an open-source molecular builder and visualization tool. Version 1.2.0. http://avogadro.cc/
37. Hanwell, M.D.; Curtis, D.E.; Lonie, D.C.; Vandermeersch, T.; Zurek, E.; Hutchison, G.R.; Avogadro: An advanced semantic chemical editor, visualization, and analysis platform. J. Cheminformatics. 2012, 4, 17.
38. Molecular Operating Environment (MOE), Version 2018.01. http://www. chemcomp.com